

www.acsami.org Research Article

# Improved Recovery of Captured Airborne Bacteria and Viruses with **Liquid-Coated Air Filters**

Daniel P. Regan, ChunKi Fong, Avery C. S. Bond, Claudia Desjardins, Justin Hardcastle, Shao-Hsiang Hung, Andrew P. Holmes, Jessica D. Schiffman, Melissa S. Maginnis, and Caitlin Howell\*



Cite This: ACS Appl. Mater. Interfaces 2022, 14, 50543-50556



**ACCESS** I

Metrics & More

Article Recommendations

Supporting Information

ABSTRACT: The COVID-19 pandemic has revealed the importance of the detection of airborne pathogens. Here, we present composite air filters featuring a bioinspired liquid coating that facilitates the removal of captured aerosolized bacteria and viruses for further analysis. We tested three types of air filters: commercial polytetrafluoroethylene (PTFE), which is well known for creating stable liquid coatings, commercial high-efficiency particulate air (HEPA) filters, which are widely used, and in-house-manufactured cellulose nanofiber mats (CNFMs), which are made from sustainable materials. All filters were coated with



omniphobic fluorinated liquid to maximize the release of pathogens. We found that coating both the PTFE and HEPA filters with liquid improved the rate at which Escherichia coli was recovered using a physical removal process compared to uncoated controls. Notably, the coated HEPA filters also increased the total number of recovered cells by 57%. Coating the CNFM filters did not improve either the rate of release or the total number of captured cells. The most promising materials, the liquid-coated HEPA, filters were then evaluated for their ability to facilitate the removal of pathogenic viruses via a chemical removal process. Recovery of infectious JC polyomavirus, a nonenveloped virus that attacks the central nervous system, was increased by 92% over uncoated controls; however, there was no significant difference in the total amount of genomic material recovered compared to that of controls. In contrast, significantly more genomic material was recovered for SARS-CoV-2, the airborne, enveloped virus, which causes COVID-19, from liquid-coated filters. Although the amount of infectious SARS-CoV-2 recovered was 58% higher, these results were not significantly different from uncoated filters due to high variability. These results suggest that the efficient recovery of airborne pathogens from liquid-coated filters could improve air sampling efforts, enhancing biosurveillance and global pathogen early

KEYWORDS: airborne pathogens, aerosol filtration, HEPA, bioaerosols, SARS-CoV-2

### 1. INTRODUCTION

Frequent collection and identification of airborne pathogens can assist with monitoring high-risk environments such as travel hubs, hospitals, and other public spaces while also helping to fill critical gaps in our current knowledge of aerosol transmission routes. Furthermore, robust biosurveillance systems can track mutations and shifts in the genomics and proteomics of spreading pathogens<sup>4</sup> and even help to guard against catastrophic spreading situations in enclosed environments, such as the International Space Station and future human habitations on the moon and Mars, where bioaerosol dynamics and microbial growth are much different from that on Earth. Critically, knowledge of the presence of airborne pathogens will continue to become increasingly important as changing climate patterns drive a shift in microbial distribution.

To gain information about bioaerosols, two main types of samplers are typically used, depending on the deployment environment and desired analysis.8 Liquid impingers are used when maintaining pathogen viability is desired; unfortunately, these platforms face issues of sample loss, reaerosolization, and

low capture efficiency. 9,10 Alternatively, filter-based sampling is used when the particle size and treatment volume are the important variables; however, factors such as desiccation and impaction impair the viability of captured pathogens. 10,11 To address this issue and increase pathogen viability and transfer for analysis, researchers have modified filter-based sampling using gelatin filters. Although promising, this approach is still faced with a lack of stability that limits the operational parameters to short use, even in moderate temperatures. 12 Further approaches have involved the consideration of how other types of filtration media such as granulated activated carbon might be adapted to reduce the disintegration of delicate biological particles, such as through altering bulk density and hardness. 13 Nevertheless, new approaches, which

Received: August 16, 2022 Accepted: October 25, 2022 Published: November 4, 2022





preserve viability while permitting the treatment of larger volumes to compensate for low concentrations, are needed.

While not a conventional means of air sampling, highefficiency particulate air (HEPA) filters play a critical role in infection control strategies.2 One study that tested the use of portable HEPA filtration units in a simulated COVID isolation room found that the volume treatment rates reached upwards of 20 air changes per hour, greater than the recommended 12, while capturing 98% of the surrogate aerosols. 15 Others have shown that HEPA filters can significantly reduce the burden of airborne fungi, 16 bacteria, 17 and viruses, 15,18 including SARS-CoV-2.<sup>19</sup> Given the widespread availability of HEPA filters, particularly in the wake of the COVID-19 pandemic, it stands to reason that filter-based methods will continue to play a large role in future air purification. However, it is recognized that recovering infectious viruses or live bacteria, as opposed to only ribonucleic acid (RNA), is more challenging, <sup>20,21</sup> particularly with HEPA filters. <sup>22</sup> Therefore, a method of easily collecting infectious viruses and/or living bacteria is needed to enable increased access to important sample information.

Over the past decade, immiscible liquid coatings on solid surfaces, otherwise known as liquid-infused surfaces, have demonstrated their strong potential for the handling and manipulation of biological samples, <sup>23</sup> including bacteria, <sup>24–28</sup> proteins, <sup>29</sup> and biological fluids, <sup>30</sup> both in vitro and in vivo. <sup>31–33</sup> These systems consist of a material substrate and an infusing liquid, associated via chemical affinity, to repel immiscible liquids. 34,35 Recently, the approach of adding an immobilized liquid layer to a solid substrate has also been applied to filtration materials to produce either liquid-gated membranes, in which the liquid reversibly fills the pores, 36-39 or liquid-coated membranes, in which the pores remain open. 40 Most of these studies have used commercial polytetrafluoroethylene (PTFE) filters that were coated with a perfluoropolyether (PFPE) oil. 36,39,41 Liquid-coated filters have primarily been studied as a filter for multiphase separations, <sup>37,39,42</sup> preventing fouling of inorganic matter, <sup>37,41</sup> increasing flux recovery against organic foulants, 19 and improving the durability of filters for water treatment.<sup>3</sup> However, to date, no study has investigated the application of liquid-coated filter surfaces for airborne pathogen collection and recovery.

In this work, we demonstrate how liquid-coated filters, which we refer to as liquid nets (LNs), can be used to first trap airborne bacteria- and virus-containing droplets under 5  $\mu$ m in diameter and subsequently release the pathogen for culture analysis more easily than uncoated filters. We use three different filter types: PTFE, chosen for its high chemical affinity for the coating liquid; HEPA, chosen for its ubiquity in current commercial filtration systems; and CNFM, chosen for its sustainability. Our goal was to examine the ability of these three types of filters, both with and without the LN coating, to release Escherichia coli collected from airborne droplets. We further aimed to test the most promising LN system against airborne viral particles, examining the ability of our systems to release infectious viral particles as well as total viral genetic information, as tracking where pathogens are infectious versus simply present can be a key piece of information in public health response planning. We demonstrate that when added to common commercial filtration materials, particularly HEPA filters, LNs can enhance the capture of airborne pathogens for analysis. To the best of our knowledge, this is the first time that liquid-coated materials have been used to assist in the intentional capture and release of biological agents and provide a new tool for the global community to more quickly and accurately track the spread of pathogens and other biological

### 2. EXPERIMENTAL METHODS

2.1. Filter Sourcing and Preparation. 2.1.1. Materials and Chemicals. All chemicals and materials were used as received.

Unlaminated 1.0  $\mu$ m PTFE filters were purchased from Sterlitech Corp, and melt-blown polypropylene H13 HEPA filters were purchased from the Nanjing Blue Sky Filter Co. The Krytox PFPE coating liquids were purchased from DuPont through Fisher Scientific. Novec 7100 Engineered fluid was purchased from Sigma-Aldrich. Cellulose acetate ( $M_w = 30\,000$  Da by GPC,  $\geq 97\%$ ) and paraformaldehyde (PFA) were purchased from Sigma-Aldrich (St. Louis, MO). Acetone (histological grade), sodium hydroxide (NaOH, ACS), ethanol (absolute anhydrous), and phosphate-buffered saline (PBS) were obtained from Fisher Scientific (Fair Lawn, NJ). Deionized water was obtained from a Barnstead Nanopure Infinity water purification system (Thermo Fisher Scientific, Waltham, MA). DAPI (4',6-diamidino-2-phenylindole) nuclear stain and the secondary Alexa Fluor antibodies were also sourced from Thermo Fisher. SARS-CoV-2 NP antibodies were sourced from Sino Biological (Beijing, China). MEM and DMEM cell culture media was obtained from Corning (New York, NY). Water dye for the sliding angle tests, FD&C Yellow #5, and FD&C Blue #1 were obtained from Hannaford Supermarkets, Orono, ME. Triton X-100 was purchased from Millipore Sigma (Burlington, MA), Tween from Biotium (Fremont, CA), goat serum from Vector Laboratories (Burlingame, CA), and binding buffer from IDEXX (Westbrook, ME).

2.1.2. Fabrication of Electrospun Cellulose Nanofiber Mats (CNFMs). The procedure used to manufacture the cellulose nanofibers was based on our prior publication. 43 Cellulose acetate (2.25 g) was dissolved in 15 mL of acetone (15% w/v) under ambient conditions using an Arma-Rotator A-1 (Bethesda, MA) mixing at 20 rpm for 24 h. This precursor solution was loaded into a 5 mL Luer-Lock tip syringe capped with an 18-gauge needle that was mounted on a PHD Ultra syringe pump (Harvard Apparatus, Plymouth, PA). Using alligator clips, a high-voltage supply (Gamma High Voltage Research Inc., Ormond Beach, FL) was connected to the needle and to the collector (a copper plate wrapped with aluminum foil). The electrospinning apparatus parameters were held constant and included a flow rate of 3 mL/h, an applied voltage of 25 kV, and a separation distance of 10 cm. During production, a temperature of 22 ± 1 °C and a relative humidity of 22% were maintained using a desiccant unit (Drierite, Xenia, OH) inside of an environmental chamber (CleaTech, Santa Ana, CA). Cellulose acetate nanofiber mats were electrospun for 30 min before being removed from the collector and sandwiched between Chemical-Resistant Slippery Teflon PTFE Sheets (3.2 mm × 101.6 mm × 152.4 mm, McMaster-Carr, Robbinsville, NJ) to be converted into CNFMs. The as-spun mats were thermally treated for 1 h at 208 °C, followed by submersion in a 0.1 M NaOH solution (4:1 v/v of water/ethanol) for 16 h, and washed 3 times with deionized water before being placed in a desiccator overnight at room temperature. To ensure that the samples were uniform, the bulk thickness of each CNFM was measured at three different locations on every sample using a Mitutoyo 293-330 digital micrometer (Toronto, Ontario, Canada). CNFM with a thickness of 50  $\mu$ m was used throughout this study.

2.1.3. Preparation of LNs on Filters. All base filters were cut into circles with a 1.7 cm diameter (surface area 2.27 cm<sup>2</sup>). A Krytox K103 PFPE was added dropwise on top of the filters until the minimum volume to visibly wet the entire membrane was achieved. Samples were hung vertically for at least 30 min to ensure that no excess oil remained on the filters.

2.2. LN Characterization and Performance Assessment. 2.2.1. LN Characterization. Contact angle and sliding angle measurements (n = 3) were conducted, as previously described.<sup>40</sup> Liquid layer stability was analyzed by submerging the samples in an aqueous 0.1% crystal violet (CV) solution (n = 5 for each treatment) and incubating for 10 min. Samples were then removed from the CV solution and washed thoroughly in deionized water. Excess water was removed using the corner of a Kimwipe without touching the surface of the samples. Images were taken with controlled lighting with an EOS 5D Mark II camera (Canon). Percent CV coverage, a proxy for the absence of the liquid coating, was conducted in ImageJ (NIH). Scanning electron microscopy (SEM) images were captured on an AMRay 1820 set to 10 kV. Prior to imaging, dry control filters were mounted with adhesive carbon tapes on aluminum stubs. The samples were then sputter-coated (Cressington) with gold—palladium until the coating was 4 nm thick.

2.2.2. Performance of Air Filters to Remove Particulate Matter. All filters investigated, including CFNM, PTFE, and HEPA, were punched into 2.54 cm diameter disks using a Spearhead 130 Power Punch MAXiSET (Fluid Sealing Services, Wausau, WI) to fit the testing instrument. For CNFM and PTFE air filters, three 50 µm thick disks were stacked to achieve a total thickness of 150  $\mu$ m before the liquid infusion to be consistent with our previous work. 43 Particulate matter was generated by simultaneously burning three Hem Precious Chandan incense sticks (Hicksville, NY) in a custom-built chamber to mimic extremely hazardous air quality, with a PM concentration >2000  $\mu g/m^3$  (>2 × 10<sup>5</sup> particles/cm<sup>3</sup>) (see Figure S1). A model 3775 condensation particle counter (CPC, TSI Incorporated, Shoreview, MN) and a Series 3080 electrostatic classifier (TSI Incorporated, Shoreview, MN) at a sample flow rate of 3.0 L/m were used to measure the downstream particle concentration and particle size distribution from 20 to 900 nm. These two instruments operate together as a scanning mobility particle sizer (SMPS) and quantify the particle number based on discrete particle size ranges. A custom-built filter module was used to hold the air filter sample in line with a vacuum pump (face velocity = 15.1 cm/s) using the choked flow induced by a brass critical orifice (size 4, O'Keefe Controls Co., Trumbull, CT). A digital pressure gauge (SSI Technologies, LLC, Janesville, WI) was used to measure the differential pressure across the filter. The effective filter area was 5 cm<sup>2</sup>, and all filters were tested for 20 min (after allowing the particle concentration to stabilize for 10 min). Downstream particles were analyzed during the last 10 min of the test to evaluate the filter performance, such as filtration efficiency (E, see eq 1) and quality factor (QF, see eq 2). In eq 1,  $C_{up}$  and  $C_{down}$ are the number of particle counts at the filter upstream and downstream, respectively, whereas in eq 2,  $\Delta P$  is the pressure drop across the filter

$$E = 1 - \frac{C_{\text{down}}}{C_{\text{up}}} \tag{1}$$

$$QF = \frac{\ln(1 - E)}{\Delta P} \tag{2}$$

**2.3.** Preparation of Stock Solutions for Bioaerosol Generation. *2.3.1.* Bacterial Stocks. Stock solutions of E. coli EMG2 with the protein expression plasmid pBBR-MCS5 GFP in 2 mL of Luria Broth (LB) Miller containing 5  $\mu$ g/mL of gentamicin sulfate were prepared in a shaker incubator (MaxQ 6000, Thermo Fisher Scientific) at 37 °C and 100 rpm for 20 h. Serial dilutions of the stock were conducted in a 1 × phosphate-buffered solution (PBS) and adjusted to an optical density at 600 nm (GENESYS 10S UV–vis, Thermo Fisher Scientific) of 0.04 A relative to the 1 × PBS blank. This corresponded to a starting concentration between 10<sup>5</sup> and 10<sup>6</sup> colony-forming units (CFUs)/mL.

2.3.2. Viral Stocks. 2.3.2.1. JCPyV Stock and Host Cells. SVGA cells were cultured in complete minimum essential medium (MEM) with 10% fetal bovine serum (FBS), 1% penicillin–streptomycin (Mediatech, Inc.), and 0.2% plasmocin (InvivoGen). Cells were propagated in a humidified incubator at 37 °C with 5% CO<sub>2</sub> and were passaged 2–3 times weekly. SVGA cells were graciously donated by the Atwood Laboratory (Brown University); JCPyV strain Mad-1/SVE $\Delta$  was also provided by the Atwood Laboratory (Brown University). Growth and preparation of JCPyV supernatant stock

were described previously.<sup>46</sup> In brief, four roller bottles (Corning, 1750 cm<sup>2</sup>) of SVGA cells at 70% confluence were infected with ICPvV until significant cytopathic effects (CPEs) were observed. Cells were scraped into the supernatant and transferred into 500 mL centrifuge bottles. After centrifugation, pellets were resuspended in 10 mL of MEM and aliquoted into 50 mL conical tubes. Samples underwent three freeze/thaw cycles at −80 °C to lyse cells and then were sonicated. Deoxycholate (in diH2O) was added to a final concentration of 0.25% (in MEM), and lysates were incubated in a 37 °C water bath for 30 min. Centrifugation at 10 000 RPM was performed for further clarification of the virus supernatant. The supernatant was collected and stored at −80 °C. JCPyV stock was titred by the fluorescent focus unit (FFU) infectivity assay in SVGA cells using a Nikon Eclipse Ti epifluorescence microscope (Micro Video Instruments, Inc.). The final stock concentration was 1.66 × 10<sup>7</sup> FFU/mL.

2.3.2.2. SARS-CoV-2 Stock and Host Cells. All SARS-CoV-2 procedures were performed under BSL-3 conditions. The following reagent was deposited by the Centers for Disease Control and Prevention and obtained through BEI Resources, NIAID, NIH: SARS-related coronavirus 2, isolate hCoV-19/USA/OR-OHSU-PHL00037/2021 (Lineage B.1.1.7;  $\alpha$ -variant), and NR-55461. SARS-CoV-2 was propagated using an established procedure<sup>47</sup> with some modifications as described below. Vero E6 cells were obtained through ATCC (no. CRL-1586) and maintained in complete Dulbecco's modified Eagle's medium (DMEM) containing 10% FBS, 1% penicillin-streptomycin, and 0.2% plasmocin. The cells were propagated in a humidified incubator at 37 °C with 5% CO<sub>2</sub> and were passaged 2-3 times weekly. The cells were seeded in T-75 flasks to reach a 90% confluence. At the time of infection, 50  $\mu$ L of SARS-CoV-2 (BEI Resources) was diluted into 5 mL of serum-free DMEM and added to a T-75 flask. The flask was incubated at 37 °C for 30 min, rocking every 10 min. After 30 min, 10 mL of complete DMEM was added to the flask, and the flask was incubated for 72 h. At 72 hpi, upon the observation of significant CPE, the cell monolayer was scraped and the contents of the flask were pipetted into conical tubes. The viral lysate underwent three freeze-thaw cycles at -80 and 37 °C, respectively, and the supernatant was clarified by centrifugation. The clarified virus supernatant was aliquoted into tubes and stored at -80 °C. The virus was titered using a TCID<sub>50</sub> assay, as previously described by Stanifer et al.  $^{48}$  The final stock concentration was 1.1 imes10<sup>5</sup> TCID<sub>50</sub>/mL.

**2.4. Filtration of Bioaerosols.** Aerosolization of the pathogen-containing solutions was conducted in the dead-end filtration setup detailed in Figure S2. The aerosol generation devices were housed in the aerosol chamber, a modified 19.7 cm diameter vacuum desiccator (Bel-Art). Negative pressure was pulled across the filters placed in a QF-16 stainless steel housing (Kurt J. Lesker Co.) and obtained using a PV-35 vacuum pump (Precision Scientific Co.). Transfilter pressure was monitored using a pressure gauge (SMC), and bypassed aerosol droplets were collected in a vacuum trap and Dewar flask (Chemglass Life Sciences). For all experiments, an alternating order of dry control and coated filters was used to minimize any change due to the accumulation of pathogen-containing aerosols within the chamber.

2.4.1. Bacterial Aerosols. For E. coli-containing solutions, a volume of 80 mL of the bacterial stock described in Section 2.3 was placed in an ultrasonic diffuser (InnoGear), which was expected to produce bacteria-containing aerosol droplets with a median aerodynamic diameter of  $1.8 \pm 1.6 \ \mu m$ . Prior to running the first filter, a 15 min priming cycle was conducted with the vacuum and diffuser running to equilibrate the system. Next, a filter was placed in the system and a three-phase process was followed to ensure the maximum capture of the bioaerosol: first, a 1 min cycle under vacuum (only) was performed to deform the liquid around the pores. Second, a 6 min aerosolization stage including the ultrasonic diffuser and vacuum was run. Third, the diffuser was turned off while the vacuum remained on for 1 min to clear the aerosol chamber.

2.4.2. Viral Aerosols. A commercial mesh nebulizer (Philips Innospire Go) was used to accommodate small volumes of virus-containing liquids. This device was expected to produce aerosols with

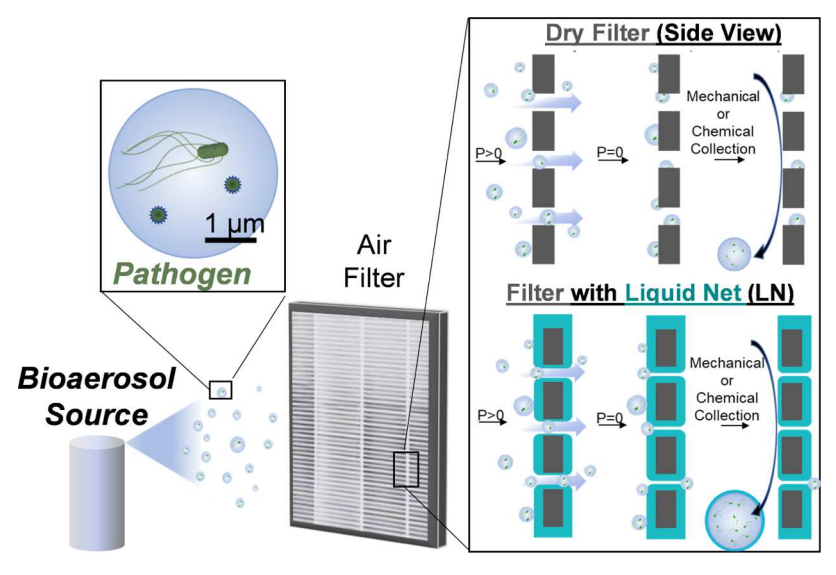


Figure 1. Schematic representation of the recovery of pathogen-containing aerosols using dry filters vs LNs.

an average mean aerodynamic diameter of  $3.99 \pm 0.26 \ \mu m$ . <sup>50</sup> Only HEPA filters (liquid-coated or dry, n=5) were used for these experiments due to their better performance in testing with bacteria-containing aerosols. A volume of 0.5 mL JCPyV or SARS-CoV-2 viral stock described in Section 2.3 was placed into the nebulizer and run until all of the stock was depleted or after 1 min, whichever came first.

**2.5. Pathogen Collection and Analysis.** 2.5.1. Collection of Bacterial Aerosols. After filtration cycles had been run, the filters were removed from the housing and placed into a conical tube for 15 min. Collection of *E. coli* from the filters was accomplished by physically impressing (stamping) onto LB Miller agar plates containing 5  $\mu$ g/mL of gentamicin sulfate by applying pressure by sweeping curved forceps over the entire filter. Care was taken to ensure that the pressure applied during each cycle was held as constant as possible. Each filter was cycled through this removal process nine consecutive times. Plates were then incubated at 37 °C for 24 h before conducting CFU counts. Normalized CFU count ( $N_{CFU}$ ) was calculated as

$$N_{\rm CFU} = \frac{U_{\rm N}}{U_{\rm l}} \tag{3}$$

where  $U_{\rm N}$  is the CFU count at the removal cycle N, and  $U_{\rm 1}$  is the CFU count at the first removal cycle. It is important to note that the percent recovery was not calculated due to loss of an unknown quantity of the pathogen to the walls of the containment vessels.

2.5.2. Collection and Analysis of Viral Aerosols. Following filtration, filters were allowed to rest for 15 min before being transferred into a conical tube containing 0.5 mL of a hydrofluoroether Novec 7100 Engineering Fluid (fluorinated phase) and 1 mL of PBS (aqueous phase) and manually shaken for 1 min to remove the virions from the HEPA filter. The extraction fluid was then allowed to separate for 5 min before analysis. Blank PBS and Novec were analyzed as negative controls, while the original viral stock was used as a positive control.

2.5.2.1. JCPyV  $\dot{R}$ T-PCR. The DNA from JCPV was directly extracted from the viral samples using the DNeasy Blood & Tissue Kit (Qiagen), according to the manufacturer's protocol. Immediately following extraction, samples were analyzed by qPCR in triplicate on the Bio-Rad CFX 96 thermal cycler, using the Bio-Rad CFX Manager software 4.1. Each reaction included 10  $\mu$ L of iQ SYBR green Supermix (Bio-Rad), 0.03  $\mu$ L of VP1 forward primer (IDT), 0.03  $\mu$ L of VP1 reverse primer (IDT), 6.9  $\mu$ L of nuclease-free water, and 3  $\mu$ L of viral DNA extract for a total reaction volume of 20  $\mu$ L per well on Hard-Shell 96-well PCR plates (Bio-Rad). The plates were sealed with Microseal "B" seals (Bio-Rad). The cycling conditions used were previously described 51 with a modification to 35 cycles.

2.5.2.2. JCPyV Infectivity Assay. SVGA cells were seeded in 96-well plates in complete MEM to achieve 70% confluence. Cells were infected with 23  $\mu$ L/well of each sample in triplicate wells and equal amounts of complete MEM to provide cell nutrients. Infection plates were incubated at 37 °C for 1 h. Cells were fed with 100  $\mu$ L/well of complete MEM and incubated at 37 °C for 72 h. At 72 hpi, cells were fixed with 4% paraformaldehyde (PFA), washed with PBS, and stained by indirect immunofluorescence for the nuclear expression of JCPyV VP1.

2.5.2.3. JCPyV Indirect Immunofluorescence. All 96-well plates were washed 3× with PBS-T for 5 min. Cells were permeabilized with 1% Triton X-100 in PBS at RT for 15 min and then blocked with 10% goat serum in 0.01% PBS-Tween (PBS-T) at room temperature (RT) for 1 hr. A primary antibody against JCPyV VP1 (PAB597) (1:40) in PBS-T was added at 50  $\mu$ L/well at RT for 1 h. Wells were washed 3× with PBS-T for 5 min. Secondary polyclonal goat antimouse Alexa Fluor 594 antibody (1:1000) in PBS-T was added at 50  $\mu$ L/well at RT for 1 h. Wells were washed 3× with PBS-T for 5 min. DAPI (1:1000) in PBS-T was added at 50  $\mu$ L/well at RT for 5 min for visualization of cell nuclei. Wells were washed 3× with PBS-T for 5 min, and 200  $\mu$ L/well of PBS was added for storage. Infection was quantified by averaging the number of VP1-positive nuclei per 20X visual field for five fields of view per well using a Nikon Eclipse Ti epifluorescence microscope (Micro Video Instruments, Inc.).

2.5.2.4. SARS-CoV-2 RT-PCR. SARS-CoV-2 RNA was directly extracted using the water DNA/RNA Magnetic Bead Kit (IDEXX), with several modifications to the manufacturer's protocol. First, a working solution was created using 250  $\mu$ L of binding buffer, 25  $\mu$ L of proteinase K, and 20  $\mu$ L of magnetic beads per sample. Then, 295  $\mu$ L of working solution was added to each 1.5 mL microcentrifuge tube, along with 100 µL of sample. Each tube was briefly vortexed and incubated at 58 °C for 10 min. The rest of the extraction process adhered to the manufacturer's protocol. Following extraction, samples were analyzed by qPCR in triplicate on the Bio-Rad CFX 96 thermal cycler, using the reagents from the water SARS-CoV-2 RT-PCR Test (IDEXX). Each reaction included 10  $\mu$ L of SARS-CoV-2 Mix, 10  $\mu$ L of RNA MMix, and 5 µL of viral RNA extract. The qPCR cycling conditions consisted of an initial reverse transcription step of 50 °C for 15 min, a denaturation step of 95 °C for 1 min, followed by 45 cycles of the amplification step of 95 °C (15 s) and 60 °C (30 s). The FAM reporter was used for SARS-CoV-2 detection, with ROX as the passive reference.

2.5.2.5. SARS-CoV-2 Infectivity Assay. Vero E6 cells were seeded in 96-well plates in complete DMEM to achieve 70% confluence at the time of infection. In the BSL-3 facility, cells were infected with 23  $\mu$ L/well of each sample in triplicate wells and equal amounts of

Table 1. Characteristics of the Three Filter Types Used in This Work

Filter Type	Filter Chemistry	Dry Contact Angle (°)	Coating Liquid Chemistry	Loading (µL/cm²)	Tilt Angle (°)
PTFE	F F	132.6 ± 3.3		15.3 ± 1.8	8.5 ± 3.0
HEPA	$ \begin{bmatrix} CH_3 \\ CH-CH_2 \end{bmatrix}_{n} $	89.4 ± 22.8	$F_3C = O - CF - CF_2 - O + CF_2 - O - CF_3$	56.2 ± 3.6	No sliding up to 45°
CNFM	HO OH OH OH	0.1 ± 0.0		17.6 ± 1.4	No droplet; complete wetting

complete DMEM to provide cell nutrients. Infection plates were incubated at 37 °C for 1 h. Cells were fed with 100  $\mu$ L/well of complete DMEM and incubated at 37 °C for 24 h. At 24 hpi, cells were fixed with 4% paraformaldehyde (PFA), washed with PBS, and stained by indirect immunofluorescence for the cellular expression of cytoplasmic SARS-CoV-2 nucleocapsid.

2.5.2.6. SARS-CoV-2 Indirect Immunofluorescence. All 96-well plates were washed 3× with PBS-T for 5 min and then permeabilized with 1% Triton X-100 in PBS for 15 min at RT. Primary antibody against SARS-CoV-2 nucleocapsid (NP) (Sino Biological) (1:500) in PBS-T was added at 50  $\mu$ L/well at RT for 1 h. Wells were washed 3× with PBS-T for 5 min. Secondary polyclonal goat antimouse Alexa Fluor 488 antibody (1:1000) in PBS-T was added at 50  $\mu$ L/well at RT for 1 h. Wells were washed 3× with PBS-T for 5 min. DAPI (1:1000) in PBS-T was added at 50  $\mu$ L/well at RT for 5 min for visualization of cell nuclei. Wells were washed 3× with PBS-T for 5 min, and 200  $\mu$ L/well of PBS-T was added for storage. Infection was quantified by counting the number of NP-positive cells per well using a Nikon Eclipse Ti epifluorescence microscope.

**2.6. Statistical Analysis.** *2.6.1. Filter Performance Analysis.* One-way ANOVAs were used to assess the performance of the filters, with significance determined using Tukey HSD post hoc tests.

2.6.2. Bacterial Aerosol Analysis. For analysis of the bacteria-containing aerosols, a 2 × 2 × 2 ANOVA (R studio) with 95% confidence intervals was performed to analyze statistical significance between the LNs (comparing recovery duration, volume of infusing liquid, and viscosity of infusing liquid). Mann—Whitney U-tests (R Studio or Graphpad Prism) were performed to determine the statistical significance between the CFU recovery from the dry control and the LN samples.

2.6.3. Viral Aerosol Analysis. For viral infectivity assays, Kruskal—Wallis tests were used as the data were not normally distributed, where P values of < 0.05 were considered statistically significant. For the data generated by triplicate qPCR reactions, Mann—Whitney Utests were used (Graphpad Prism), again to account for unequal variance among the samples. All plots were made using Microsoft Excel software.

### 3. RESULTS AND DISCUSSION

Our goal was to create liquid net (LN) systems in which pathogens would be easy to remove, as the liquid surface and pathogen-containing droplets would more easily come away from the base filter than the pathogen-containing droplets alone, as shown schematically in Figure 1. To test this hypothesis, three different types of filters were coated with PFPE liquids: PTFE-LNs, HEPA-LNs, and CNFM-LNs. A relatively low-viscosity (82 cSt) PFPE liquid, Krytox 103, was chosen as the coating liquid in all cases as this fluorinated material has been shown to result in highly stable layers that are resistant to both oil- and water-based foulants. <sup>23,34</sup> For the filters, PTFE was chosen as it has been used extensively in

conjunction with PFPE to create stable liquid-coated surfaces for a wide range of applications. <sup>23,34,53</sup>

HEPA filters were selected due to their ubiquity in air filtration applications, importance as part of the COVID-19 pandemic response, and wide commercial availability. <sup>22,54</sup> Finally, CNFMs were tested as they have been previously shown to be effective in air filtration applications and are made from biodegradable cellulose, <sup>43</sup> an increasingly interesting material in light of the ongoing efforts to improve environmental sustainability. <sup>55,56</sup>

**3.1. Filter Characterization.** LN samples were fabricated as described in the Experimental Methods section from three different types of filtration materials: commercially available PTFE and HEPA filters, as well as in-house-manufactured CNFMs. A comparison of the three different filter types both before and after coatings is given in Table 1. As expected, the contact angles for the three types of filters prior to coating reflected their known characteristics: PTFE was confirmed to be hydrophobic, HEPA was borderline hydrophobic and highly variable, and CNFM was superhydrophilic with full wetting of the membrane occurring immediately upon contact with the water droplet. Once coated with the PFPE liquid, the filters were tested for the minimum angle at which a water droplet would slide across the surface, as a proxy for the intactness and functionality of the liquid coating.<sup>57</sup> PTFE-LNs showed a low tilt angle, consistent with previous reports on similar systems. <sup>23,34,58</sup> The stability of PFPE liquids on PTFE surfaces is known to be due to a combination of chemical matching between the solid material and the liquid coating as well as contributions from capillary forces, resulting in a robust and extremely slippery surface. <sup>23,34</sup> Tests on the characterization of PTFE-LNs with different loading volumes and different PFPE coating liquid viscosity liquids were also tested with similar results; the results are given in Table S1. The HEPA-LNs, in contrast, showed sticking of the droplet up to, and including at 45°, the maximum angle tests. The lack of droplet sliding indicates either a dewetting of the coating liquid from the fiber surface upon contact with the water droplet, which is likely due to the mismatch between the surface chemistry of the polypropylene fibers of the HEPA filter and the PFPE liquid, or fiber features larger than the thickness of the liquid coating. 59,60 It is also possible that the results are due to some combinations of these two. The CNFM-LNs also had no measurable tilt angle, but unlike the HEPA-LNs, on which the droplet was present but unmoving, this was due to the droplet displacing the PFPE liquid and absorbing it into the filter itself.

**3.2. Filter Performance Analysis.** To assess if the coating liquid affected the filtration efficiency, we performed an analysis of particle filtration efficiency, pressure drop, and

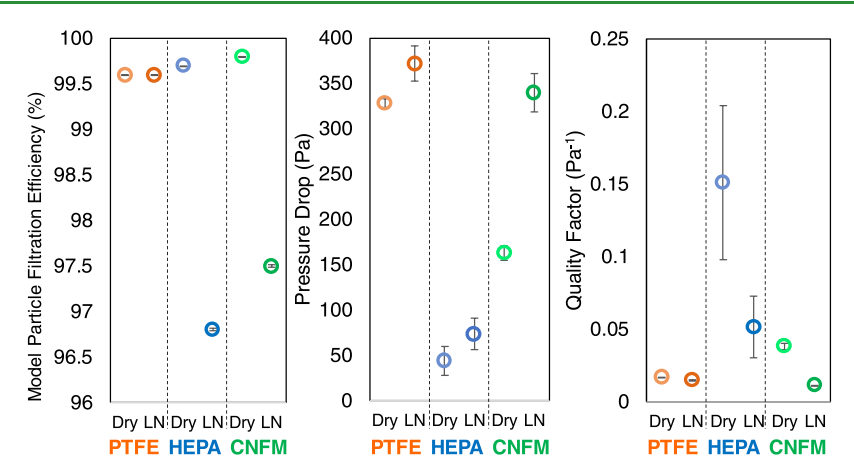


Figure 2. Measurements of the filtration efficiency (left), pressure drop (center), and quality factor (right) for different membranes (cellulose nanofiber mats [CNFMs], polytetrafluoroethylene [PTFE], high-efficiency particulate air [HEPA]) either dry (uncoated) or coated with liquid (liquid nets, LNs) at a flow rate of 3.0 L/m.

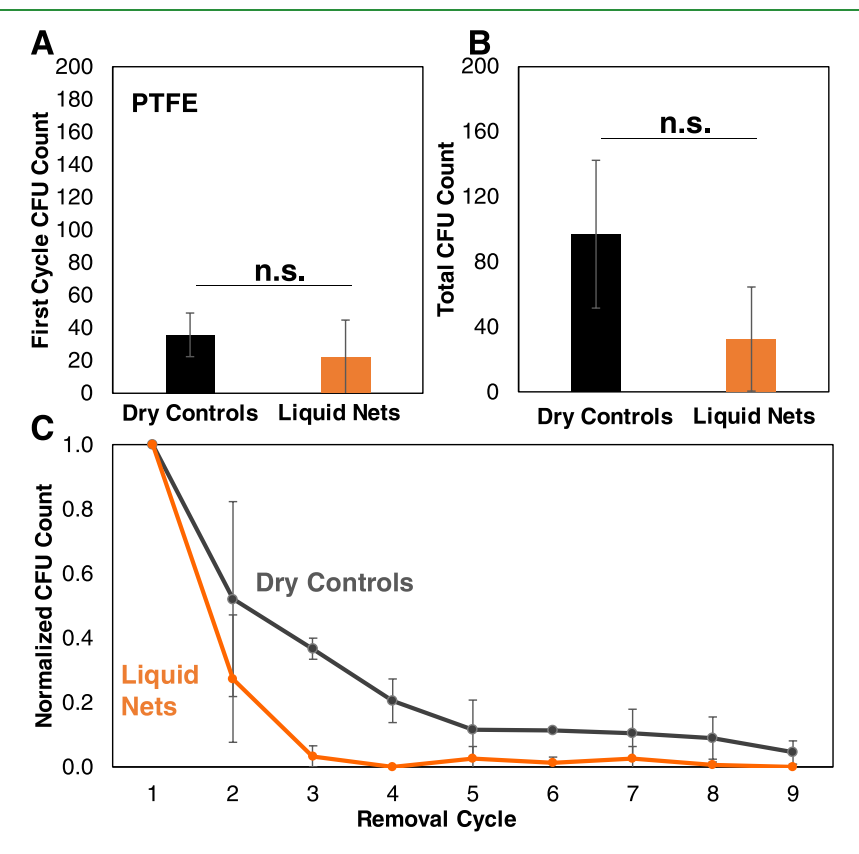


Figure 3. Effect of PTFE-LNs on the recovery of aerosolized bacteria. Cumulative colony-forming unit (CFU) count of (A) the first removal cycle and (B) the total of all nine removal cycles for dry PTFE controls (dark gray) versus liquid nets (LNs) made with PFPE liquid. (C) Number of CFUs released from the filter during each removal cycle (stamp onto agar plate). Values are normalized to the number obtained from the first cycle, the bacteria removal cycle, for direct comparison. All error bars represent standard deviations; n = 3 for all data points; n.s. signifies no statistical significance.

filtration quality factor. While the wetting behavior of the test aerosol can lead to different collection phenomena, in this work we focused on changing the collection media while holding the particulate matter (PM) chemistry constant. Coated and uncoated PTFE, HEPA, and CNFM filters were tested by generating hazardous air quality that contained a high PM concentration of >2000  $\mu$ g/m³ (see Figure 2). The testing chamber was covered with tar after testing, suggesting that burning incense to generate the particles yields oily droplets, as expected. The PTFE-LNs showed no significant differences in

either filtration efficiency (p = 0.719) or pressure drop (p = 0.0876) when coated with an LN and a statistically significant decrease in the quality factor (p = 0.0114). Some differences between the PTFE and PTFE-LNs are expected due to the slight average narrowing of the pores upon introduction of the liquid coating to the system or even complete blocking of some of the pores. The HEPA- and CNFM-LNs, however, showed marked decreases in particle filtration efficiency and quality factor and simultaneous increases in pressure drop. This is likely due to the increased chemical mismatch between the

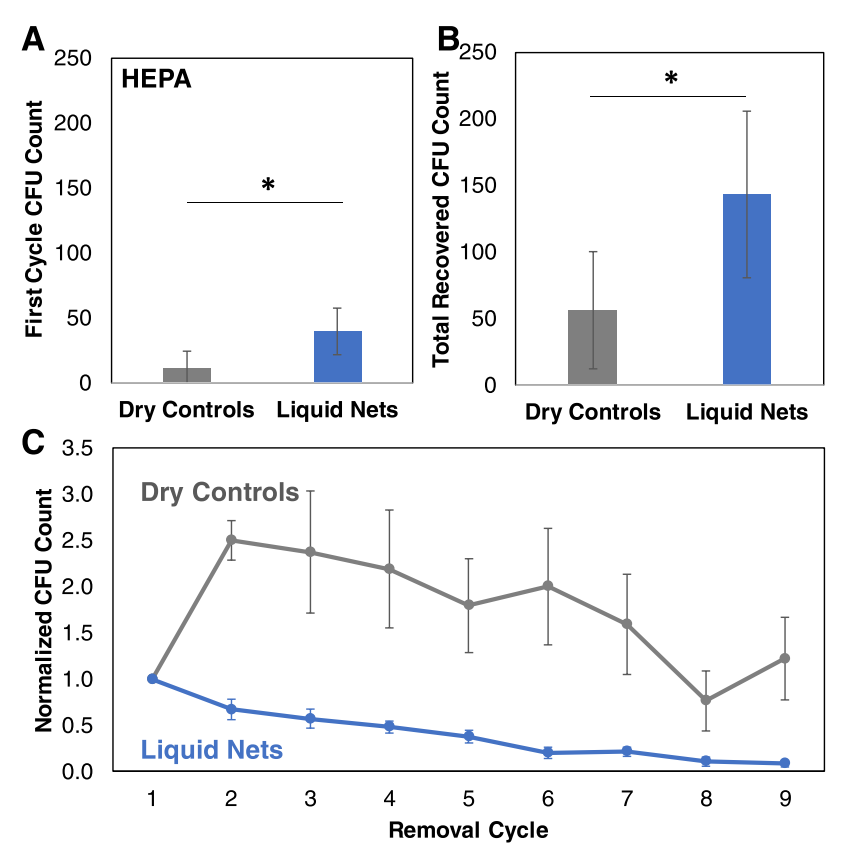


Figure 4. Effect of HEPA-LNs on the recovery of aerosolized bacteria. Colony-forming unit (CFU) count of (A) the first removal cycle and (B) the total of all nine removal cycles for dry HEPA control filters (dark gray) vs HEPA-LNs (blue). (C) Normalized release rate for each bacteria removal cycle. (C) Number of CFUs released from the filter during each removal cycle (stamp onto agar plate). Values are normalized to the number obtained from the first cycle, the bacteria removal cycle, for direct comparison. All error bars represent standard deviations; n = 6; \* signifies statistical significance at P < 0.05.

chemistry of the base filter material (polypropylene for HEPA and cellulose for CNFM) and the fluorinated PFPE coating liquid, which would make it easier for the thin liquid coating to be deformed within the pores or otherwise displaced from the solid substrate. The HEPA filters show the largest decrease in filtration efficiency and quality factor when coated to create HEPA-LNs. This could be due to the additional effect of the coating liquid dissipating the charge on the polypropylene fibers, which serve to enhance filtration efficiency in untreated HEPA filters. It has been reported that the removal efficiency is greater when oily particles are used as the PM, for example, when cellulose fiber aerogels functionalized with silane groups were evaluated. Nevertheless, it appears that coating filters to create LNs alters the filtration capacity.

**3.3. Recovery of Bacteria from Aerosols.** *3.3.1. PTFE-LNs.* PTFE is a commonly used commercial material in air filtration due to its stability and fouling resistance. The ability of PTFE-LNs and dry control PTFE filters to release aerosolized *E. coli* onto culture plates via surface stamping over several cycles was investigated. The results are shown in Figure 3. There were no significant differences in the total amount of bacteria recovered after the first removal cycle (Figure 3A), nor the total amount of bacteria released after all nine removal cycles (Figure 3B) between the PTFE-LNs and the dry PTFE controls. One reason for this lack of difference may be that the PTFE filters themselves are designed to be antifouling and so adding a thin LN to an already antiadhesive surface has little to no effect on the overall recovery. Furthermore, previous work

with silicone-based liquid-coated surfaces demonstrated that microdroplets containing *E. coli* can actually become entrapped in a liquid layer due to embedding and formation of the wrapping layer over the droplets. <sup>65</sup> A similar phenomenon may be occurring here.

However, further investigation showed that some differences between the controls and the PTFE-LNs were apparent. Figure 3C shows the normalized number of CFUs recovered  $(N_{CFU})$ after nine sequential "stamp" removal cycles to remove the captured bacterial cells. Values are presented as normalized to the CFU number from the first stamp for direct comparison. The data show that the  $N_{CFU}$  per cycle approached zero more quickly for the PTFE-LNs compared to that for dry controls, with a significant difference emerging at the third removal cycle (P = 0.0005). Similar results were found for PTFE-LNs made with different viscosity PFPE coating liquids and higher liquid loading volumes (Figure S3). The faster decrease in  $N_{CFU}$ suggests a faster rate of removal despite a similar quantity of removal. This might be because after the first removal cycles, the PFPE liquid layer itself begins to be removed. As these liquids are not covalently bound to the PTFE surface, both the liquid and the pathogens they contain are more easily separated from the solid filter substrate than pathogens remaining on the solid surface of the controls.

3.3.2. HEPA-LNs. Given the importance of HEPA filters in air filtration and purification applications, tests were conducted to determine if adding LNs to these materials could also enhance the recovery of bacteria-containing aerosols using the

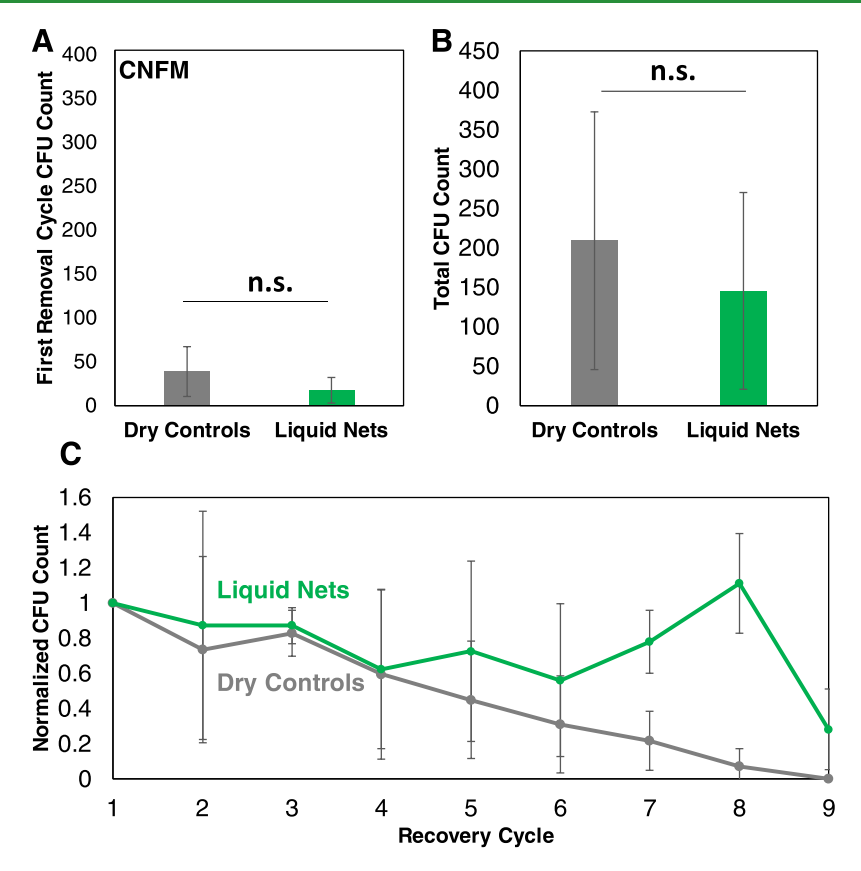


Figure 5. Effect of CNFM-LNs on the recovery of aerosolized bacteria. Colony-forming unit (CFU) counts from (A) just the first removal cycle and (B) the total CFU collected over nine removal cycles from dry cellulose nanofiber mat (CNFM) control filters (dark gray) vs CNFM coated with the lower-viscosity liquid (green). There were no significant differences among the samples. (C) Normalized CFUs released from the dry CNFM controls and CNFM liquid nets (LNs) at each removal cycle. All error bars represent standard deviations; n = 3; n.s. signifies no statistical significance.

same mechanical stamp method used for the PTFE filters. Figure 4 shows the results of the aerosol capture analysis for the HEPA-LNs vs dry HEPA controls. CFU counts from the first removal cycle (Figure 4A) showed a significant increase in the number of viable bacteria that could be removed from the HEPA-LN compared to that of the dry HEPA control (P =0.015), while the total cumulative CFU count over all nine removal cycles (Figure 4B) also showed a significantly greater number of cells recovered from the LN (P = 0.025). Figure 4C shows the normalized CFU removal,  $N_{CFU}$ , over each of the nine cycles. The dry HEPA controls consistently show values over or near 1 with large error bars, indicating that the number of CFUs being recovered at each cycle was highly variable and that the cells were not easily removed from the surface. In contrast, the HEPA-LNs showed normalized CFU values always below 1 and approaching 0 by the final removal cycle, with small error bars. This is indicative of bacterial cells being more easily and more reproducibly removed from the surface, with the near-total recovery of the available cells occurring by the final cycle.

The recovery of significantly more CFUs from HEPA-LNs both in the first removal cycle and in total over nine removal cycles likely indicates that the coating liquid itself is coming away from the HEPA surface more easily. It is well known that coating liquids that chemically match their solid substrates will completely wet those substrates and remain associated with them, resisting displacement by other liquids. However, recent work has shown that even imperfectly matched liquid—

substrate pairs can create functional, stable liquid coatings under flow conditions.<sup>40</sup> The imperfectly matched polypropylene of the HEPA membrane and the PFPE liquid used in this system may therefore be creating a coating layer that is stable enough for filtration but unstable enough to be easily removed.

3.3.3. CNFM-LNs. Given the promising results of increased *E. coli* recovery on the HEPA-LNs despite their liquid—solid chemical mismatch, we investigated LNs fabricated with another type of mismatched filter: electrospun CNFMs. CNFM-LNs were fabricated by coating in-house-manufactured CNFMs with low-viscosity PFPE at a loading volume of 17.6  $\mu$ L/cm<sup>2</sup>. As with the HEPA-LNs, analysis of the sliding angle showed that a water droplet placed on these surfaces would not slide down at any angle up to and including 45°, indicating the lack of a continuous, molecularly smooth liquid overlayer and/or topographical roughness impeding droplet movement.

The results of the bacterial aerosol capture tests using CNFM-LNs are shown in Figure 5. No significant differences relative to dry CNFM controls were observed for either the first recovery cycle (Figure 5A) or the total amount of recovered cells over all nine recovery cycles (Figure 5B). Analysis of  $N_{\rm CFU}$  released from both filter types over each of the nine mechanical stamping removal cycles showed a large variation in the number of recovered cells for both the dry controls and CNFM-LMs (Figure 5C). Unlike the PTFE- and HEPA-LNs, the addition of the liquid coating to the CNFM filters did not appear to enhance the recovery of the bacteria from the surface. In fact, the dry controls showed what

appeared to be improved recovery over time, as the CFU values for those samples approached 0, while the CFU values for the CNFM-LNs continued to fluctuate around 1, indicating that all available bacterial cells were not being efficiently removed.

The observed lack of improved bacterial recovery from CNFM-LNs was not surprising given the greater mismatch between the cellulose fibers and the PFPE coating liquid. Unlike the HEPA filters, which presented a hydrophobic, though not fluorinated, surface for association with the PFPE coating liquid, the cellulose fibers are highly hydrophilic. Any aqueous droplet that comes in contact with a PFPE-coated cellulose fiber will easily displace the coating liquid, while droplets coming into contact with a PFPE-coated polypropylene fiber may or may not displace the coating, depending on other forces at play in the environment.<sup>57</sup> In case the aqueous droplets do displace the coating on the polypropylene fibers, it is more likely that they will detach easily from these hydrophobic materials than they would a hydrophilic cellulose surface, as the droplet contact area decreases on hydrophobic surfaces.

3.4. Filter Characterization and Comparison. To further investigate the stability of the liquid coating on the three types of membranes, we tested the stability of the liquid coating by immersing the coated filters in a 0.01% crystal violet (CV)-in-water staining solution for 10 min. If the coating was stable, we would expect to see none of the CV dye adhering to the surface. In contrast, if the PFPE liquid coating was easily displaced by the CV solution, we anticipated seeing a deeply stained filter.40

Figure 6A shows the results of the staining tests on the PTFE-, HEPA-, and CNFM-LNs compared to those on dry

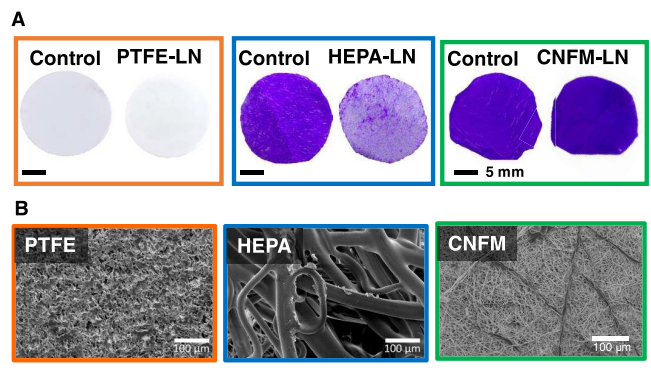


Figure 6. Analysis of liquid coating integrity and dry filter surface. (A) Filters both with and without LNs after immersion in crystal violet stain. The LN coating prevents the CV from binding to the filter surface, providing an indicator of where the coating liquid is present and where it is not. (B) SEM images of a PTFE, HEPA, and CNFM filter surface.

controls. No staining was observed on either the PTFE dry controls or PTFE-LNs, in agreement with their known antifouling nature.<sup>34</sup> After immersion of the HEPA filters into CV, the dry control was nearly completely stained (93.3  $\pm$ 3.9% CV coverage), while the HEPA-LN showed significantly less coverage (P-value < 0.001) at only 15.8  $\pm$  6.4%. In contrast, both the CNFM dry controls and the CNFM-LNs were completely stained (100% CV coverage) after the removal from the stain solution. These results support the hypothesis that the liquid coating on the HEPA-LNs was more

stable when exposed to an aqueous solution compared to that on the CNFM-LNs, which was completely or near-completely displaced.

SEM images of the surfaces of the dry control filters were collected (Figure 6B). The results showed much larger fibers on the surface of the HEPA filters compared to either the PTFE or CNFM materials, in agreement with previous reports on the characterization of these systems. 43,66 It is known that the stability of liquid coatings is due not only to a chemical match between the surface and coating liquid but also to the capillary action. The difference in the CV staining results obtained for the HEPA-LNs may therefore be due to an increased contribution of capillary forces to holding the liquid coating in place, further explaining their better performance in the recovery of bacterial aerosols.

3.5. Recovery of Viruses from Aerosols. The notable increase in the recovery of viable bacterial cells from aerosols using HEPA-LN was promising, and the mechanism of action suggested that this approach could be applied to viruscontaining aerosols as well. To test this, we aerosolized two different types of viruses: one nonenveloped and one enveloped. For the nonenveloped virus, we used JC polyomavirus (JCPyV), a virus that is the causative agent of the often-fatal disease progressive multifocal leukoencephalopathy (PML).<sup>67</sup> For the enveloped virus, we chose SARS-CoV-2, the virus responsible for the COVID-19 pandemic.<sup>68</sup>

To test the efficiency of HEPA-LNs for virus recovery, viral particles concentrated directly from cell culture media were aerosolized and passed through HEPA-LNs or dry HEPA controls in a setup similar to that used to collect the bacterial aerosols. Recovery of the viruses was conducted by extracting the filter in a mixture of PBS (aqueous phase) and hydrofluoroether (fluorinated phase). The collected samples were analyzed for the recovery of viral genomic material using qRT-PCR as well as the presence of infectious viruses using an indirect immunofluorescence assay of infectivity.

The qRT-PCR results for the two types of viruses are shown in Figure 7, in which a lower value indicates the presence of more genomic material, showing that there was no significant difference in the amount of JCPyV DNA recovered from the HEPA-LNs compared to that of the controls (P = 0.5806); however, a significantly greater amount of SARS-CoV-2 RNA was recovered from the filters with LNs (P = 0.0023). Interestingly, for JCPyV, significantly more DNA was recovered in the aqueous extraction phase than in the fluorinated phase for both the HEPA and HEPA-LNs (P < 0.0001). In contrast, there was no significant difference in the amount of SARS-CoV-2 RNA recovered between the aqueous and fluorinated phases for the dry HEPA controls (P =0.0756), although there was a significant increase in recovery from the HEPA-LNs in the aqueous phase compared to that in the fluorinated phase (P = 0.0243). This may indicate a difference in the way that the viruses are interacting with the fluorinated PFPE coating and the combined aqueousfluorinated extraction fluid used to recover the viral particles from the filter surfaces. JCPyV is a nonenveloped virus with a pure protein outer surface,<sup>67</sup> while SARS-CoV-2 is an enveloped virus with a combined lipid-protein outer layer. The fluorinated extraction fluid used to recover the viruses in these tests is known to solubilize light oils and so was likely interacting more with the lipid component of the SARS-CoV-2 viral particles than the JCPyV and pulling more of those particles into the fluorinated phase along with the PFPE

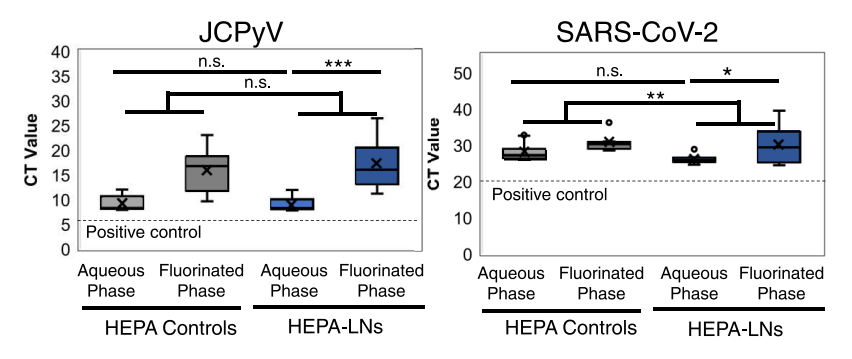


**Figure 7.** HEPA liquid nets recover JCPyV and SARS-CoV-2: qRT-PCR. Values from the viral genomic material harvested from samples from n = 9 (JCPyV) or n = 6 (SARS-CoV-2) samples collected over three or two separate runs, respectively. A lower value indicates more genomic material present. Both the aqueous and fluorinated phases of the liquid used to recover JCPyV and SARS-CoV-2 from either dry control (HEPA controls) or liquid net (HEPA-LN) filter surfaces are given. Average Ct values are represented, with \* signifying significance at P < 0.05,\*\* significance at P < 0.001. Data represent triplicate samples for three (JCPyV) or two (SARS-CoV-2) independent experiments.

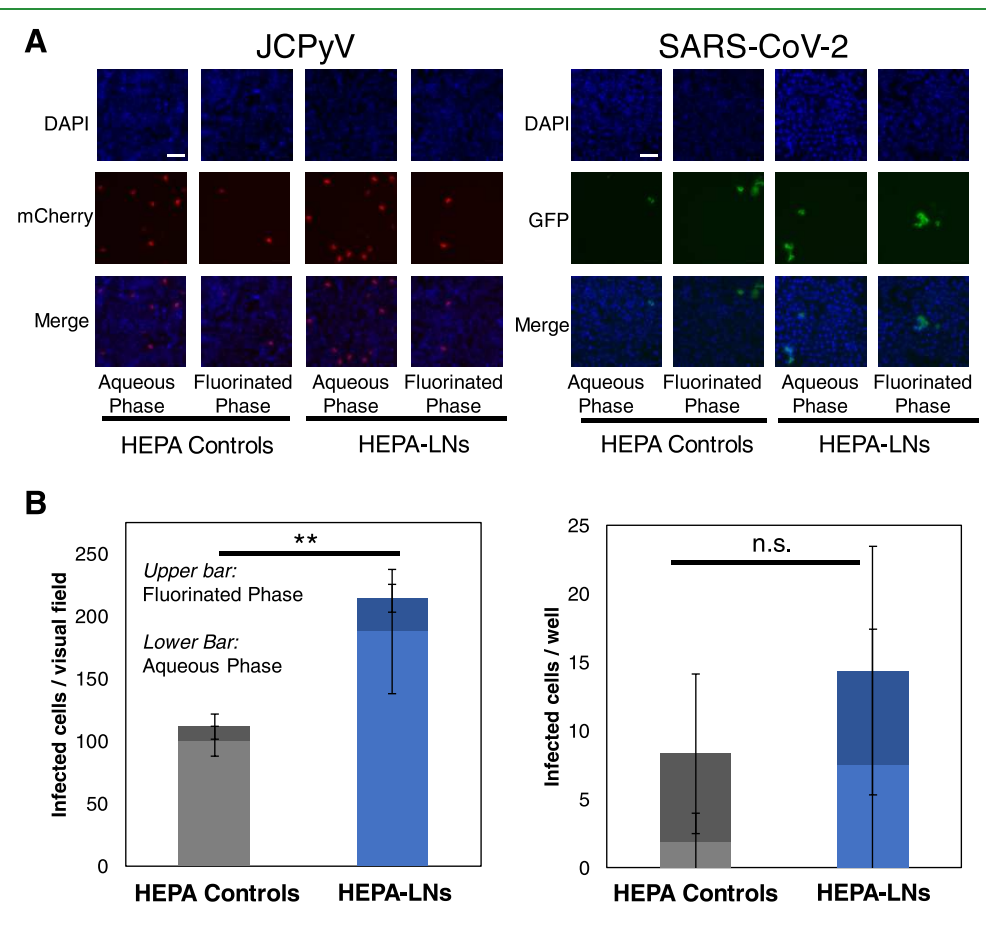


**Figure 8.** HEPA-LNs recover JCPyV and SARS-CoV-2: infectivity. Qualitative (A) and quantitative (B) infectivity results from the samples presented in Figure 6. (A) Representative images at 20× illustrate infected cells (JCPyV in red, SARS-CoV-2 in green) and total cells (blue). (B) Average number of infected cells/20× field of view normalized to 100% of the control aqueous phase sample (JCPyV) or per well (SARS-CoV-2). Data represent triplicate samples for three (JCPyV) or two (SARS-CoV-2) independent experiments. Scale bars = 100  $\mu$ m. \*\*Signifies significance at P < 0.01.

coating liquid. The JCPyV particles, however, would have preferentially associated with the aqueous phase over the fluorinated phase, explaining the significant increase in the recovered viral genomic material in that portion of the extraction fluid.

The greater effect of the fluorinated extraction fluid on SARS-CoV-2 can also be seen in the results displayed in Figure 8, which show the number of cells that were infected by the recovered sample. Both the qualitative (Figure 8A) and

corresponding quantitative (Figure 8B) infectivity results showed 92% more infectious, nonenveloped JCPyV recovered from HEPA-LNs than dry HEPA controls (P=0.0057), echoing the significant increase in the recovery of bacterial cells. The HEPA-LNs also showed a 58% increase in the recovery of SARS-CoV-2, although this result was not significant (P=0.4515) due to the large standard deviation among the samples. The high variability was likely due to the disruptive nature of the fluorinated extraction fluid on the viral

particles. If the fluorinated phase was able to solubilize more viral particles, it is also likely that it disrupted the envelope of some of those particles, rendering them noninfectious.

It is well known that liquid-based samples can preserve the infectivity of captured viruses; however, dry samplers are easier to operate and have the capacity to filter larger volumes over long periods.<sup>14</sup> Here, we have attempted to achieve some of the benefits of both by modifying dry-sampling filters with a nonevaporating, omniphobic liquid. Although the liquid coating is most likely not protecting the integrity of the viral particles in the same way that an aqueous liquid would, it may nevertheless offer some additional protection against desiccation through mechanisms that only liquid can achieve such as the formation of a wrapping layer around the aerosolized droplets. 23,59 Furthermore, the neutral pH of the PFPE liquid may additionally be helping to improve the stability of the virions.<sup>69</sup> Our results also show that the selection of coating and recovery fluids is critical to obtaining the desired outcome of collecting and protecting the pathogens until they can be analyzed. Coating/recovery fluids that interact with the pathogens themselves—likely occurring with the fluorinated recovery phase and the SARS-CoV-2 lipid envelope here—can disrupt the delicate biological structures. The size of the viral particle might also be playing a role: JCPyC is 45-50 nm, <sup>67</sup> while SARS-CoV-2 is 60-140 nm.68 However, our results suggest that the reverse might also be true: that a carefully chosen coating or extraction fluid could serve to further protect the pathogens and preserve their infectiousness or other critical properties, allowing more information to be gathered during later analysis. More work is needed to elucidate the exact mechanisms of pathogen-coating liquid-extraction process interactions and apply that knowledge to further optimization of LN technology.

There are some considerations and limitations to this study. First, it should also be noted that the concentrations of infectious viral particles in the aerosols used here are likely to be higher than in most real-world settings. For example, the maximum concentration of SARS-CoV-2 achieved in our aerosol vessel was approximately  $2.2 \times 10^5 \text{ TCID}_{50}/\text{m}^3$ , while measurements of concentration in hospital settings have yielded values in high-risk areas such as patient rooms between  $3.8 \times 10^3$  and  $7.2 \times 10^3$  TCID<sub>50</sub>/m<sup>3</sup>.<sup>70</sup> Nevertheless, air sampling for pathogens often involves a concentration step between recovery and analysis,<sup>64</sup> and something similar could also be used with the LN system. Second, we did not directly assess the percent recovery<sup>14</sup> of either our bacterial or our viral aerosols, and instead the relative recovery of our LN filters compared to their dry controls. This was due to the unknown quantity of pathogen lost within our aerosolization setup due to sticking of the droplets to the chamber and tubing walls. With our findings serving as proof of concept that the use of LNs does indeed increase pathogen recovery on commercial filtration materials, future work will focus on more in-depth characterization and improvement. Finally, the presence of the liquid coating did decrease the filtration efficiency for most of the LNs, particularly the HEPA-LNs. Thus, the tradeoffs between bioaerosol capture and recovery should be taken into account when considering the use of LN technology.

Our work has shown that the addition of LNs is effective at increasing the amount of infectious virus and/or viral genetic material that can be recovered from standard filtration materials such as the melt-blown polypropylene used in HEPA filters. To the best of our knowledge, this is the first

report on the improvement of commercial HEPA filters for the recovery of pathogens, particularly viruses that retain their infectiousness. Our findings may open doors to more widespread and frequent sampling, which can be critical in accurately assessing risk levels.

#### 4. CONCLUSIONS

The goal of this work was to create filters that could more easily release captured bioaerosols for analysis. To accomplish this, we coated common filtration materials with a fluorinated PFPE liquid to create an LN system. Three types of filters were tested: commercial fluorinated PTFE, commercial polypropylene HEPA filters, and in-house-manufactured, cellulose CNFMs. LNs formed on commercially available PTFE filters showed no significant increases in the amount of aerosolized E. coli recovered using a physical removal process; however, bacteria could be released more rapidly from liquid-coated surfaces than dry control surfaces. The recovery did not improve when either the coating viscosity or total liquid loading onto the filters was changed. LNs created on commercial polypropylene HEPA filters, however, showed a significant increase in both the total number of bacteria recovered and the rate at which the bacteria were recovered. LNs on CNFMs showed no improvement in either bacterial recovery or the rate of recovery, suggesting an important role of both filter surface chemistry and topography in the functionality of the LN systems. Additional tests using two types of viruses, nonenveloped JCPyV and enveloped SARS-CoV-2, showed that the HEPA-LNs were able to significantly increase the amount of infectious virus (for JCPyV) and total viral genetic material (SARS-CoV-2) over dry HEPA controls when using a chemical recovery method. Differences in the types and quantities of viral recovery were attributed to varying interactions of the outer surface of the viruses with the fluorinated solvent used for the chemical recovery. These results show that the addition of liquid coatings to create LNs on commercial air filtration materials can increase the amount of pathogenic material recovered for analysis.

### ASSOCIATED CONTENT

### **Solution** Supporting Information

The Supporting Information is available free of charge at https://pubs.acs.org/doi/10.1021/acsami.2c14754.

Fractional particle distribution of the upstream incense particles, images of the aerosolization setup, characteristics of LNs, and performance of PTFE-LNs as a function of oil loading are provided (PDF)

#### AUTHOR INFORMATION

#### **Corresponding Author**

Caitlin Howell - Department of Chemical and Biomedical Engineering, University of Maine, Orono, Maine 04469, United States; Graduate School of Biomedical Science and Engineering, University of Maine, Orono, Maine 04469, *United States;* orcid.org/0000-0002-9345-6642; Email: caitlin.howell@maine.edu

### **Authors**

Daniel P. Regan - Department of Chemical and Biomedical Engineering, University of Maine, Orono, Maine 04469, United States; Graduate School of Biomedical Science and

- Engineering, University of Maine, Orono, Maine 04469, United States; orcid.org/0000-0002-6363-0144
- ChunKi Fong Graduate School of Biomedical Science and Engineering, University of Maine, Orono, Maine 04469, United States
- Avery C. S. Bond Department of Molecular and Biomedical Sciences, University of Maine, Orono, Maine 04469, United States
- Claudia Desjardins Department of Molecular and Biomedical Sciences, University of Maine, Orono, Maine 04469, United States
- Justin Hardcastle Graduate School of Biomedical Science and Engineering, University of Maine, Orono, Maine 04469, United States
- Shao-Hsiang Hung Department of Chemical Engineering, University of Massachusetts Amherst, Amherst, Massachusetts 01003-9303, United States; orcid.org/0000-0001-8160-2668
- Andrew P. Holmes Cooperative Extension, University of Maine, Orono, Maine 04473, United States; ⊚ orcid.org/ 0000-0001-5012-4026
- Jessica D. Schiffman Department of Chemical Engineering, University of Massachusetts Amherst, Amherst, Massachusetts 01003-9303, United States; orcid.org/0000-0002-1265-5392
- Melissa S. Maginnis Department of Molecular and Biomedical Sciences, University of Maine, Orono, Maine 04469, United States; Graduate School of Biomedical Science and Engineering, University of Maine, Orono, Maine 04469, United States

Complete contact information is available at: https://pubs.acs.org/10.1021/acsami.2c14754

### Notes

The authors declare no competing financial interest.

### ACKNOWLEDGMENTS

The authors thank Prof. Emeritus Bill Halteman for assistance with statistical analysis and Prof. Richard E. Peltier for use of his SMPS equipment. The authors also thank Northern Light Health for the donation of critical PPE. This work was supported by the National Science Foundation award nos. 2029378 and 1939710, the University of Maine Research Reinvestment Funds, the University of Maine Graduate School of Biomedical Science and Engineering, and the Maine Space Grant Consortium Graduate Fellowship. Research in the Maginnis Laboratory was supported by the National Institute of Allergy and Infectious Diseases of the National Institutes of Health grant number R15AI144686 and funding from the University of Maine.

### ABBREVIATIONS

PFPE, perfluoropolyether PTFE, polytetrafluoroethylene HEPA, high-efficiency particulate air CNFM, cellulose nanofiber mat LN, liquid net

### **■** REFERENCES

(1) Nasir, Z. A.; Campos, L. C.; Christie, N.; Colbeck, I. Airborne Biological Hazards and Urban Transport Infrastructure: Current

- Challenges and Future Directions. *Environ. Sci. Pollut. Res.* **2016**, 23, 15757–15766.
- (2) Saran, S.; Gurjar, M.; Baronia, A.; Sivapurapu, V.; Ghosh, P. S.; Raju, G. M.; Maurya, I. Heating, Ventilation and Air Conditioning (HVAC) in Intensive Care Unit. *Crit. Care* **2020**, *24*, No. 194.
- (3) Fujiyoshi, S.; Tanaka, D.; Maruyama, F. Transmission of Airborne Bacteria across Built Environments and Its Measurement Standards: A Review. *Front. Microbiol.* **2017**, *8*, No. 2336.
- (4) Herfst, S.; Böhringer, M.; Karo, B.; Lawrence, P.; Lewis, N. S.; Mina, M. J.; Russell, C. J.; Steel, J.; de Swart, R. L.; Menge, C. Drivers of Airborne Human-to-Human Pathogen Transmission. *Curr. Opin. Virol.* **2017**, 22, 22–29.
- (5) Després, V.; Alex Huffman, J.; Burrows, S. M.; Hoose, C.; Safatov, A.; Buryak, G.; Fröhlich-Nowoisky, J.; Elbert, W.; Andreae, M.; Pöschl, U.; Jaenicke, R. Primary Biological Aerosol Particles in the Atmosphere: A Review. *Tellus B* **2012**, *64*, No. 15598.
- (6) Haines, S. R.; Bope, A.; Horack, J. M.; Meyer, M. E.; Dannemiller, K. C. Quantitative Evaluation of Bioaerosols in Different Particle Size Fractions in Dust Collected on the International Space Station (ISS). *Appl. Microbiol. Biotechnol.* **2019**, 103, 7767–7782.
- (7) Lai, K. M.; Emberlin, J.; Colbeck, I. Outdoor Environments and Human Pathogens in Air. *Environ. Health* **2009**, *8*, 1–5.
- (8) Jensen, P. A.; Schafer, M. P. Sampling and Characterization of Bioaerosols. NIOSH Man. Anal. Methods 1998, 1, 82-112.
- (9) Pan, M.; Lednicky, J. A.; Wu, C. Y. Collection, Particle Sizing and Detection of Airborne Viruses. *J. Appl. Microbiol.* **2019**, 127, 1596–1611.
- (10) Mainelis, G. Bioaerosol Sampling: Classical Approaches, Advances, and Perspectives. *Aerosol Sci. Technol.* **2020**, *54*, 496–519.
- (11) Cox, J.; Mbareche, H.; Lindsley, W. G.; Duchaine, C. Field Sampling of Indoor Bioaerosols. *Aerosol Sci. Technol.* **2020**, *54*, 572–584.
- (12) Fabian, P.; McDevitt, J. J.; Houseman, E. A.; Milton, D. K. Airborne Influenza Virus Detection with Four Aerosol Samplers Using Molecular and Infectivity Assays: Considerations for a New Infectious Virus Aerosol Sampler. *Indoor Air* **2009**, *19*, 433–441.
- (13) Jjagwe, J.; Olupot, P. W.; Menya, E.; Kalibbala, H. M. Synthesis and Application of Granular Activated Carbon from Biomass Waste Materials for Water Treatment: A Review. *J. Bioresour. Bioprod.* **2021**, *6*, 292–322.
- (14) Bhardwaj, J.; Hong, S.; Jang, J.; Han, C. H.; Lee, J.; Jang, J. Recent Advancements in the Measurement of Pathogenic Airborne Viruses. *J. Hazard. Mater.* **2021**, *420*, No. 126574.
- (15) Mousavi, E. S.; Godri Pollitt, K. J.; Sherman, J.; Martinello, R. A. Performance Analysis of Portable HEPA Filters and Temporary Plastic Anterooms on the Spread of Surrogate Coronavirus. *Build. Environ.* **2020**, *183*, No. 107186.
- (16) Eckmanns, T.; Rüden, H.; Gastmeier, P. The Influence of High-Efficiency Particulate Air Filtration on Mortally and Fungal Infection among Highly Immunosuppressed Patients: A Systematic Review. *J. Infect. Dis.* **2006**, *193*, 1408–1418.
- (17) Boswell, T. C.; Fox, P. C. Reduction in MRSA Environmental Contamination with a Portable HEPA-Filtration Unit. *J. Hosp. Infect.* **2006**, *63*, 47–54.
- (18) Akhai, S.; Mala, S.; Jerin, A. A. Understanding Whether Air Filtration from Air Conditioners Reduces the Probability of Virus Transmission in the Environment. *J. Adv. Res. Med. Sci. Technol.* **2021**, *8*, 36–41.
- (19) Liu, D. T.; Phillips, K. M.; Speth, M. M.; Besser, G.; Mueller, C. A.; Sedaghat, A. R. Portable HEPA Purifiers to Eliminate Airborne SARS-CoV-2: A Systematic Review. *Otolaryngol. Head Neck Surg.* **2022**, *166*, 615–622.
- (20) Degois, J.; Dubuis, M. E.; Turgeon, N.; Veillette, M.; Duchaine, C. Condensation Sampler Efficiency for the Recovery and Infectivity Preservation of Viral Bioaerosols. *Aerosol Sci. Technol.* **2021**, *55*, 653–664.
- (21) Alsved, M.; Widell, A.; Dahlin, H.; Karlson, S.; Medstrand, P.; Löndahl, J. Aerosolization and Recovery of Viable Murine Norovirus in an Experimental Setup. *Sci. Rep.* **2020**, *10*, No. 15941.

- (22) Zuniga-Montanez, R.; Coil Id, D. A.; Eisen, J. A.; Pechacek, R.; Guerrero, R. G.; Kim, M.; Shapiro, K.; Bischel, H. N. The Challenge of SARS-CoV-2 Environmental Monitoring in Schools Using Floors and Portable HEPA Filtration Units: Fresh or Relic RNA? PLoS One 2022, 17, No. e0267212.
- (23) Howell, C.; Grinthal, A.; Sunny, S.; Aizenberg, M.; Aizenberg, J. Designing Liquid-Infused Surfaces for Medical Applications: A Review. Adv. Mater. 2018, 30, No. 1802724.
- (24) Howell, C.; Vu, T. L.; Lin, J. J.; Kolle, S.; Juthani, N.; Watson, E.; Weaver, J. C.; Alvarenga, J.; Aizenberg, J. Self-Replenishing Vascularized Fouling-Release Surfaces. ACS Appl. Mater. Interfaces 2014, 6, 13299-13307.
- (25) Kovalenko, Y.; Sotiri, I.; Timonen, J. V.; Overton, J. C.; Holmes, G.; Aizenberg, J.; Howell, C. Bacterial Interactions with Immobilized Liquid Layers. Adv. Healthcare Mater. 2017, 6, No. 1600948.
- (26) Regan, D. P.; Lilly, C.; Weigang, A.; White, L. R.; Leclair, E. J.; Collins, A.; Howell, C. Combining the Geometry of Folded Paper with Liquid-Infused Polymer Surfaces to Concentrate and Localize Bacterial Solutions. Biointerphases 2019, 14, No. 041005.
- (27) Maccallum, N.; Howell, C.; Kim, P.; Sun, D.; Friedlander, R.; Ranisau, J.; Ahanotu, O.; Lin, J. J. J. J.; Vena, A.; Hatton, B.; Wong, T. T.-S.; Aizenberg, J. Liquid-Infused Silicone As a Biofouling-Free Medical Material. ACS Biomater. Sci. Eng. 2015, 1, 43-51.
- (28) Sotiri, I.; Tajik, A.; Ledoux, H.; Lai, Y.; Kovalenko, Y.; Nemr, C.; Alvarenga, J.; Timonen, J. V. I.; Hu, Y.; Aizenberg, J.; Howell, C.; et al. Tunability of Liquid-Infused Silicone Materials for Biointerfaces. Biointerphases 2018, 13, No. 06D401.
- (29) Sunny, S.; Vogel, N.; Howell, C.; Vu, T. L. T. L.; Aizenberg, J. Lubricant-Infused Nanoparticulate Coatings Assembled by Layer-by-Layer Deposition. Adv. Funct. Mater. 2014, 24, 6658-6667.
- (30) Sunny, S.; Cheng, G.; Daniel, D.; Lo, P.; Ochoa, S.; Howell, C.; Vogel, N.; Majid, A.; Aizenberg, J. Transparent Antifouling Material for Improved Operative Field Visibility in Endoscopy. Proc. Natl. Acad. Sci. U.S.A. 2016, 113, 11676-11681.
- (31) Andersen, M. J.; Fong, C.; La Bella, A. A.; Molina, J. J.; Molesan, A.; Champion, M. M.; Howell, C.; Flores-Mireles, A. L. Inhibiting Host-Protein Deposition on Urinary Catheters Reduces Associated Urinary Tract Infections. eLife 2022, 11, No. e75798.
- (32) Chen, J.; Howell, C.; Haller, C. A.; Patel, M. S.; Ayala, P.; Moravec, K. A.; Dai, E.; Liu, L.; Sotiri, I.; Aizenberg, M.; Aizenberg, J.; Chaikof, E. L. An Immobilized Liquid Interface Prevents Device Associated Bacterial Infection in Vivo. Biomaterials 2017, 113, 80-92.
- (33) Leslie, D. C.; Waterhouse, A.; Berthet, J. B.; Valentin, T. M.; Watters, A. L.; Jain, A.; Kim, P.; Hatton, B. D.; Nedder, A.; Donovan, K.; Super, E. H.; Howell, C.; Johnson, C. P.; Vu, T. L.; Bolgen, D. E.; Rifai, S.; Hansen, A. R.; Aizenberg, M.; Super, M.; Aizenberg, J.; Ingber, D. E. A Bioinspired Omniphobic Surface Coating on Medical Devices Prevents Thrombosis and Biofouling. Nat. Biotechnol. 2014, 32, 1134-1140.
- (34) Wong, T.-S.; Kang, S. H.; Tang, S. K. Y.; Smythe, E. J.; Hatton, B. D.; Grinthal, A.; Aizenberg, J. Bioinspired Self-Repairing Slippery Surfaces with Pressure-Stable Omniphobicity. Nature 2011, 477,
- (35) Kim, P.; Wong, T.-S.; Alvarenga, J.; Kreder, M. J.; Adorno-Martinez, W. E.; Aizenberg, J. Liquid-Infused Nanostructured Surfaces with Extreme Anti-Ice and Anti-Frost Performance. ACS Nano 2012, 6, 6569-6577.
- (36) Overton, J. C.; Weigang, A.; Howell, C. Passive Flux Recovery in Protein-Fouled Liquid-Gated Membranes. J. Membr. Sci. 2017, 539, 257-262.
- (37) Tesler, A. B.; Sheng, Z.; Lv, W.; Fan, Y.; Fricke, D.; Park, K.-C.; Alvarenga, J.; Aizenberg, J.; Hou, X. Metallic Liquid Gating Membranes. ACS Nano 2020, 14, 2465-2474.
- (38) Bazyar, H.; Javadpour, S.; Lammertink, R. G. H. On the Gating Mechanism of Slippery Liquid Infused Porous Membranes. Adv. Mater. Interfaces 2016, 3, No. 1600025.

- (39) Hou, X.; Hu, Y.; Grinthal, A.; Khan, M.; Aizenberg, J. Liquid-Based Gating Mechanism with Tunable Multiphase Selectivity and Antifouling Behaviour. Nature 2015, 519, 70-73.
- (40) Shah, R. M.; Cihanoğlu, A.; Hardcastle, J.; Howell, C.; Schiffman, J. D. Liquid-Infused Membranes Exhibit Stable Flux and Fouling Resistance. ACS Appl. Mater. Interfaces 2022, 14, 6148-6156.
- (41) Alvarenga, J.; Ainge, Y.; Williams, C.; Maltz, A.; Blough, T.; Khan, M.; Aizenberg, J. Research Update: Liquid Gated Membrane Filtration Performance with Inorganic Particle Suspensions. APL Mater. 2018, 6, No. 100703.
- (42) Sheng, Z.; Wang, H.; Tang, Y.; Wang, M.; Huang, L.; Min, L.; Meng, H.; Chen, S.; Jiang, L.; Hou, X. Liquid Gating Elastomeric Porous System with Dynamically Controllable Gas/Liquid Transport. Sci. Adv. 2018, 4, No. eaao6724.
- (43) Hung, S. H.; Bowden, J. W.; Peltier, R. E.; Schiffman, J. D. Optimizing the Packing Density and Chemistry of Cellulose Nanofilters for High-Efficiency Particulate Removal. Ind. Eng. Chem. Res. 2021, 60, 15720-15729.
- (44) Major, E. O.; Miller, A. E.; Mourrain, P.; Traub, R. G.; de Widt, E.; Sever, J. Establishment of a Line of Human Fetal Glial Cells That Supports JC Virus Multiplication. Proc. Natl. Acad. Sci. U.S.A. 1985, 82, 1257-1261.
- (45) Vacante, D. A.; Traub, R.; Major, E0. Extension of JC Virus Host Range to Monkey Cells by Insertion of a Simian Virus 40 Enhancer into the JC Virus Regulatory Region. Virology 1989, 170, 353-361.
- (46) Nelson, C. D. S.; Carney, D. W.; Derdowski, A.; Lipovsky, A.; Gee, G. V.; O'Hara, B.; Williard, P.; Dimaio, D.; Sello, J. K.; Atwood, W. J. A Retrograde Trafficking Inhibitor of Ricin and Shiga-like Toxins Inhibits Infection of Cells by Human and Monkey Polyomaviruses. mBio 2013, 4, No. e00729-13.
- (47) Harcourt, J.; Tamin, A.; Lu, X.; Kamili, S.; Sakthivel, S. K.; Murray, J.; Queen, K.; Tao, Y.; Paden, C. R.; Zhang, J.; Li, Y.; Uehara, A.; Wang, H.; Goldsmith, C.; Bullock, H. A.; Wang, L.; Whitaker, B.; Lynch, B.; Gautam, R.; Schindewolf, C.; Lokugamage, K. G.; Scharton, D.; Plante, J. A.; Mirchandani, D.; Widen, S. G.; Narayanan, K.; Makino, S.; Ksiazek, T. G.; Plante, K. S.; Weaver, S. C.; Lindstrom, S.; Tong, S.; Menachery, V. D.; Thornburg, N. J. Severe Acute Respiratory Syndrome Coronavirus 2 from Patient with Coronavirus Disease, United States. Emerging Infect. Dis. 2020, 26, 1266.
- (48) Stanifer, M. L.; Kee, C.; Cortese, M.; Zumaran, C. M.; Triana, S.; Mukenhirn, M.; Kraeusslich, H. G.; Alexandrov, T.; Bartenschlager, R.; Boulant, S. Critical Role of Type III Interferon in Controlling SARS-CoV-2 Infection in Human Intestinal Epithelial Cells. Cell Rep. 2020, 32, No. 107863.
- (49) Rodes, C.; Smith, T.; Crouse, R.; Ramachandran, G. Measurements of the Size Distribution of Aerosols Produced by Ultrasonic Humidification. Aerosol Sci. Technol. 1990, 13, 220-229.
- (50) Slator, L.; Degtyareva, Y.; Hardaker, L.; von Hollen, D.; Pritchard, J.Comparison of Aerosol Particle Size Measured by Two Methods Using Three Brands of Mesh Nebulizer. In Journal of Aerosol Medicine and Pulmonary Drug Delivery; Mary Ann Liebert, INC: 140 Huguenot Street, 3rd FL, New Rochelle, NY 10801 USA, 2017; Vol. 30, pp A4-A5.
- (51) Chapagain, M. L.; Verma, S.; Mercier, F.; Yanagihara, R.; Nerurkar, V. R. Polyomavirus JC Infects Human Brain Microvascular Endothelial Cells Independent of Serotonin Receptor 2A. Virology **2007**, *364*, *55*–*63*.
- (52) DuShane, J. K.; Wilczek, M. P.; Mayberry, C. L.; Maginnis, M. S. ERK Is a Critical Regulator of JC Polyomavirus Infection. J. Virol. 2018, 92, No. e01529-17.
- (53) Sotiri, I.; Overton, J. C. J. C.; Waterhouse, A.; Howell, C. Immobilized Liquid Layers: A New Approach to Anti-Adhesion Surface for Medical Applications. Exp. Biol. Med. 2016, 241, 909-918. (54) Curtis, L. HEPA Filters and Airborne Viruses, Bacteria, and

- (55) Ghisellini, P.; Cialani, C.; Ulgiati, S. A Review on Circular Economy: The Expected Transition to a Balanced Interplay of Environmental and Economic Systems. *J. Cleaner Prod.* **2016**, *114*, 11–32.
- (56) Carpenter, A. W.; De Lannoy, C. F.; Wiesner, M. R. Cellulose Nanomaterials in Water Treatment Technologies. *Environ. Sci. Technol.* **2015**, 49, 5277–5287.
- (57) Daniel, D.; Timonen, J. V. I.; Li, R.; Velling, S. J.; Aizenberg, J. Oleoplaning Droplets on Lubricated Surfaces. *Nat. Phys.* **2017**, *13*, 1020–1025.
- (58) Sotiri, I.; Overton, J. C.; Waterhouse, A.; Howell, C. Immobilized Liquid Layers: A New Approach to Anti-Adhesion Surfaces for Medical Applications. *Exp. Biol. Med.* **2016**, 241, 909–
- (59) Sett, S.; Yan, X.; Barac, G.; Bolton, L. W.; Miljkovic, N. Lubricant-Infused Surfaces for Low-Surface-Tension Fluids: Promise versus Reality. *ACS Appl. Mater. Interfaces* **2017**, *9*, 36400–36408.
- (60) Kim, P.; Kreder, M. J.; Alvarenga, J.; Aizenberg, J. Hierarchical or Not? Effect of the Length Scale and Hierarchy of the Surface Roughness on Omniphobicity of Lubricant-Infused Substrates. *Nano Lett.* **2013**, *13*, 1793–1799.
- (61) Liu, T.; Cai, C.; Ma, R.; Deng, Y.; Tu, L.; Fan, Y.; Lu, D. Super-Hydrophobic Cellulose Nanofiber Air Filter with Highly Efficient Filtration and Humidity Resistance. *ACS Appl. Mater. Interfaces* **2021**, *13*, 24032–24041.
- (62) Dhanumalayan, E.; Joshi, G. M. Performance Properties and Applications of Polytetrafluoroethylene (PTFE)—a Review. *Adv. Compos. Hybrid Mater.* **2018**, *1*, 247–268.
- (63) Shim, E.; Jang, J. P.; Moon, J. J.; Kim, Y. Improvement of Polytetrafluoroethylene Membrane High-Efficiency Particulate Air Filter Performance with Melt-Blown Media. *Polymers* **2021**, *13*, 4067.
- (64) Rahmani, A. R.; Leili, M.; Azarian, G.; Poormohammadi, A. Sampling and Detection of Corona Viruses in Air: A Mini Review. *Sci. Total Environ.* **2020**, *740*, No. 140207.
- (65) Jiang, J.; Zhang, H.; He, W.; Li, T.; Li, H.; Liu, P.; Liu, M.; Wang, Z.; Wang, Z.; Yao, X. Adhesion of Microdroplets on Water-Repellent Surfaces toward the Prevention of Surface Fouling and Pathogen Spreading by Respiratory Droplets. ACS Appl. Mater. Interfaces 2017, 9, 6599–6608.
- (66) Alassod, A.; Xu, G. Comparative Study of Polypropylene Nonwoven on Structure and Wetting Characteristics. *J. Text. Inst.* **2021**, *112*, 1100–1107.
- (67) Atkinson, A. L.; Atwood, W. J. Fifty Years of JC Polyomavirus: A Brief Overview and Remaining Questions. *Viruses* **2020**, *12*, 969.
- (68) Hu, B.; Guo, H.; Zhou, P.; Shi, Z. L. Characteristics of SARS-CoV-2 and COVID-19. *Nat. Rev. Microbiol.* **2021**, *19*, 141–154.
- (69) Hao, X.; Chen, J.; Xu, M.; Zheng, H.; Li, X.; Wang, M.; Liu, T. Separation and Purification of Enveloped and Non-Enveloped Viruses from Water Samples Using an Aqueous Two-Phase System. *Process Biochem.* **2022**, *119*, 58–67.
- (70) Birgand, G.; Peiffer-Smadja, N.; Fournier, S.; Kerneis, S.; Lescure, F. X.; Lucet, J. C. Assessment of Air Contamination by SARS-CoV-2 in Hospital Settings. *JAMA Network Open* **2020**, 3, No. e2033232.

## **□** Recommended by ACS

### Antiviral Electrospun Polyamide Three-Layered Mask Filter Containing Metal Oxide Nanoparticles and Black Seed Oil

Nourhan M. Deyab, Nageh K. Allam, et al.

NOVEMBER 17, 2022

ACS OMEGA

READ 🗹

### Nanotechnology Transition Roadmap toward Multifunctional Stimuli-Responsive Face Masks

Anna Zakrzewska, Filippo Pierini, et al.

SEPTEMBER 26, 2022

ACS APPLIED MATERIALS & INTERFACES

READ 🗹

### **Lignin: A Sustainable Antiviral Coating Material**

Alice Boarino, Francesco Stellacci, et al.

OCTOBER 13, 2022

ACS SUSTAINABLE CHEMISTRY & ENGINEERING

READ [7

### Development of Bioderived Alternatives to N95 Face Masks in a Remote Course-Based Undergraduate Research Experience

Elizabeth E. Karlsson, Aleksandr V. Zhukhovitskiy, et al.

AUGUST 22, 2022

JOURNAL OF CHEMICAL EDUCATION

READ 🗹

Get More Suggestions >